Dalton Transactions

ROYAL SOCIETY OF CHEMISTRY

PAPER

View Article Online
View Journal | View Issue

Cite this: *Dalton Trans.*, 2024, **53**, 17263

O,S-Chelated bis(pentafluorophenyl)boron and diphenylboron-β-thioketonates: synthesis, photophysical, electrochemical and NLO properties†‡

Anna Chandrasekar Murali, [a] Rudrashish Panda,[b] Ramkumar Kannan, [a] Ritwick Das *[b,c] and Krishnan Venkatasubbaiah *[a]

Boron-β-diketonates are classical emissive materials that have been utilized in various fields, however, boron monothio-β-thioketonates, where one oxygen atom is exchanged for a sulphur atom, have not been explored in detail. To gain a better understanding of this class of materials, we synthesised various aryl substituted monothio-β-diketonate boron complexes with two different aryl substitutions on the boron center and studied their structural, optical and electrochemical properties. Single crystal X-ray analysis revealed that there is considerable deviation in B–O and B–S bond lengths for bis(pentafluorophenyl)boron complexes against diphenyl boron complexes. The bis(pentafluorophenyl)boron complexes have a relatively high absorption coefficient over diphenyl boron complexes. More importantly, a striking difference was observed for the emission behaviour of these compounds. The bis(pentafluorophenyl) boron complexes exhibit weak emission in the solution as well as in the solid state, whereas diphenyl boron complexes do not show any emission in either solution or the solid state. Further, the electrochemical study reveals that diphenyl boron complexes show a reduction potential that is more negative compared to the bis(pentafluorophenyl)boron complexes. The high absorption coefficient of the compounds pointed towards the possibility of high first order hyperpolarizability upon optical excitation, which motivated us to ascertain the nonlinear optical coefficients in the near infrared range, towards applicability of such compounds in optical limiting and switching. The open aperture *Z*-scan measurements at ultrashort time scales elucidated a few critical features of such compounds towards optical limiting applications.

Received 30th August 2024,
Accepted 23rd September 2024

DOI: 10.1039/d4dt02471k

rsc.li/dalton

Introduction

Tetra-coordinated boron based molecules have attracted significant attention in different research areas such as photovoltaics, organic light-emitting diodes, sensors, and organic field-effect transistors.[1–20] Owing to their high quantum yields and high molar absorption co-efficient, boron-β-diketonates have been explored as sensors, photochromic materials, multiphoton materials, semiconductors, and polymers.[21–36] A minor alteration of boron-β-diketonates culminates in a large variation in the properties.[37,38] As a consequence, different strategies have been followed to alter the photophysical properties of boron-β-diketonates; exchange of one oxygen or two oxygen atoms in the β-diketonates with different heteroatoms has been explored by different groups. For example, the Chujo group and Gardinier group explored the photophysical properties of boron-β-ketoiminate and/or diiminates.[39,40] Recently, we reported the synthesis of boron-monothio-β-diketonates, and their non-linear optical properties and semiconducting behaviour.[17,41] The effect of substituents on the monothio-β-diketonate was explored, keeping bis(pentafluorophenyl)boron as the chelating motif. It was realized that variation of the R-group on the boron-centre (R_2B-) also influences the HOMO and LUMO levels of the molecules, and thus

[a]*School of Chemical Sciences, National Institute of Science Education and Research (NISER), an OCC of Homi Bhabha National Institute, Bhubaneswar-752050, Odisha, India. E-mail: krishv@niser.ac.in*
[b]*School of Physical Sciences, National Institute of Science Education and Research (NISER), an OCC of Homi Bhabha National Institute, Bhubaneswar-752050, Odisha, India*
[c]*Optics and Photonics Centre, Indian Institute of Technology Delhi, Hauz Khas, New Delhi-110060, India*

†This article is dedicated to Professor V. Chandrasekhar on the occasion of his 65th birthday.

‡Electronic supplementary information (ESI) available: General information, experimental details, NMR spectra, X-ray data and DFT studies. CCDC 2380850–2380854. For ESI and crystallographic data in CIF or other electronic format see DOI: https://doi.org/10.1039/d4dt02471k

helps to tune the photophysical properties.[42] This encouraged us to investigate boron monothio-β-diketonates by varying the pentafluorophenyl group with a phenyl group. Herein, we report O,S-chelated bis(pentafluorophenyl) and diphenyl organoboranes of monothio-β-diketonates, their linear and non-linear optical properties and also electrochemical properties.

Results and discussion

The bis(pentafluorophenyl)boron monothio-β-diketonates **1** to **4** and diphenylboron monothio-β-diketonates **5** to **8**, were synthesized by refluxing tris(pentafluorophenyl)borane and triphenylborane with respective starting materials **L1–L4** in dry toluene at 110 °C (Scheme 1). The starting materials **L1–L4** were prepared *via* Claisen ester condensation using NaH in DMF; a methodology similar to the one previously reported in the literature.[17,41] All the starting materials (**L1–L4**) and the boron complexes **1–8** were analysed using NMR spectroscopy, HRMS and X-ray studies (in the case of **1** to **5**). The ^{1}H-NMR analysis of starting materials **L1–L4**, show a singlet for the enolic proton in the chemical shift region of 15–16 ppm. The absence of this enolic proton peak in **1–8** suggests the emergence of the boron chelated compounds. All the bis(pentafluorophenyl)boron complexes **1–4** showed a signal attributed to $^{11}B\{^{1}H\}$ at ~1–2 ppm, and di(phenyl)boron complexes **5–8** at ~6–7 ppm, corroborating the formation of tetra-coordinated boron. The $^{19}F\{^{1}H\}$ NMR spectra of complexes **1–4** revealed three sets of peaks from ~−163.0 to −134.0 ppm, owing to the distinct environment of fluorine atoms (*ortho*, *meta*, and *para*) associated with $-B(C_6F_5)_2$.

X-ray diffraction structural analysis

Crystallization of **1–4** from a dichloromethane/*n*-hexane mixture and **5** from a chloroform/*n*-hexane mixture provided O,S-chelated boron complexes. Suitable crystals of **1–4** were crystallized in the $P\bar{1}$ space group whereas **5** was crystallized in the $P21/c$ space group. Representative structural parameters (bond angles and bond lengths) are presented in Table 1 (Tables S3 and S4‡ for optimized DFT structure). The B–O and B–S bond length observed for complexes **1–4** are notably shorter over the bond lengths realized in complex **5** (Fig. 1 and Table 1); which suggests that the electron-withdrawing $-C_6F_5$ motif plays a vital role for the observed bond distance variation. A similar trend was realized for the DFT optimized structures of the boron complexes, that is, the B–S and B–O bond lengths are shorter for **1–4** and were elongated in **5–8**. The coordination geometry around the boron center is distorted tetrahedral and the six membered ring (C3SOB) formed by the boron chelation adopts a twisted confirmation with a boron atom deviation of 0.62 Å for **1**, 0.55 Å for **2**, 0.49 Å for **3**, 0.49 Å for **4**, and 0.57 Å for **5**.

Photophysical properties and DFT analysis

The optical properties of complexes **1–8** (Table 2 and Table S5‡) were studied in various solvents such as toluene, dichloromethane (DCM), tetrahydrofuran (THF), and acetonitrile (ACN). The results pertaining to DCM are presented in the manuscript and the data related to other solvents is given in the ESI.‡ All the boron complexes **1–8** showed two absorption bands in the range 334–467 nm with extinction coefficients ranging from 10 000–30 000 M^{-1} cm^{-1} (Fig. 2).

The absorption maxima of **3** is blue-shifted as compared to **1**, **2**, and **4**; and also **7** is blue-shifted as compared to **5**, **6**, and **8** owing to the extended conjugation present in **4** and **8** and electron donating nature of $-CH_3$ and $-OCH_3$ realized in **1**, **2**, **5** and **6**. In general, the longer wavelength band of complexes with $-B(C_6F_5)_2$ showed blue-shift over complexes with –B

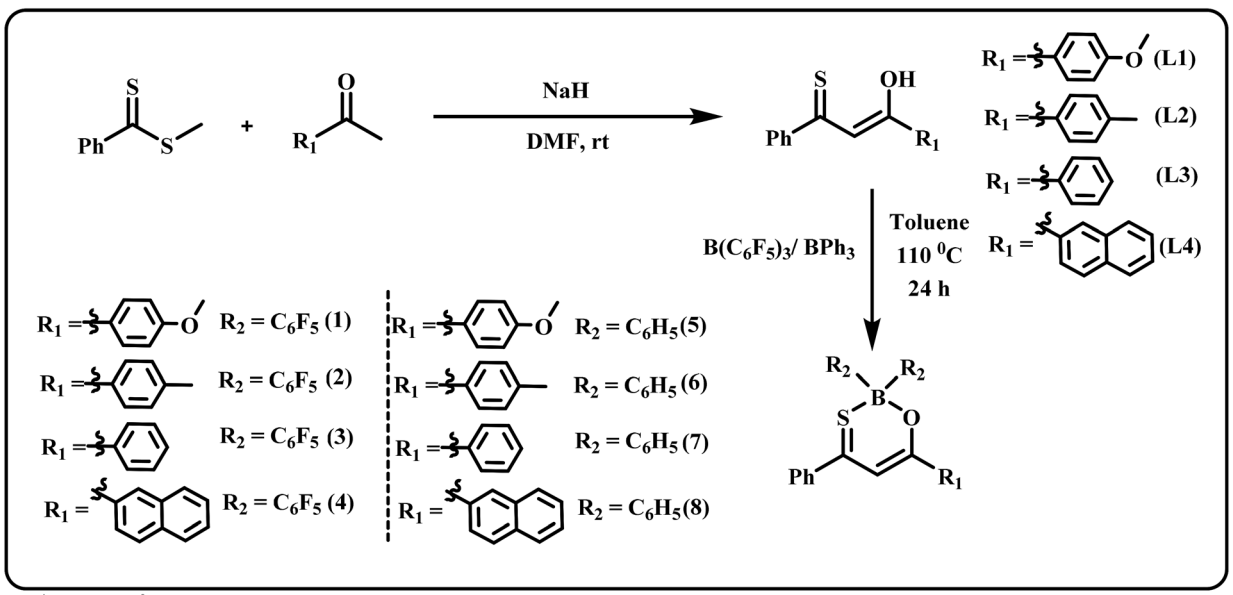

Scheme 1 Synthetic routes for **1** to **8**.

Table 1 Selected bond angles (°) and bond lengths (Å) for complexes **1–5**

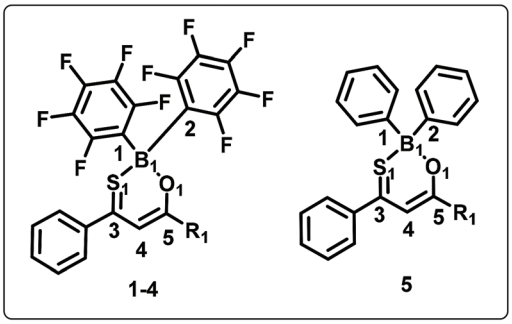

	1	2	3	4	5
S1–C3	1.718(1)	1.715(2)	1.706(2)	1.704(4)	1.706(2)
O1–C5	1.301(2)	1.295(3)	1.301(2)	1.299(4)	1.298(2)
B1–S1	1.940(2)	1.941(2)	1.949(2)	1.962(4)	1.968(2)
B1–O1	1.492(2)	1.488(3)	1.491(2)	1.496(4)	1.508(2)
B1–C1	1.616(2)	1.624(3)	1.627(2)	1.633(5)	1.603(2)
B1–C2	1.640(2)	1.641(3)	1.634(3)	1.620(5)	1.614(2)
C3–C4	1.384(2)	1.388(3)	1.387(4)	1.377(5)	1.384(2)
C4–C5	1.408(2)	1.400(3)	1.399(2)	1.397(5)	1.409(2)
S1–B1–O1	105.9(9)	106.6(1)	107.2(1)	107.1(2)	106.7(1)
S1–B1–C1	113.8(1)	112.9(1)	111.7(1)	108.6(2)	106.8(1)
O1–B1–C1	112.9(1)	113.3(2)	112.2(1)	105.7(3)	110.9(1)
C1–B1–C2	108.4(1)	109.8(2)	111.9(1)	109.4(3)	112.5(1)
C3–C4–C5	123.20(1)	123.6(2)	123.5(1)	123.1(3)	124.5(1)
B-atom deviation from C_3SOB plane (Å)	0.62	0.55	0.49	0.49	0.57

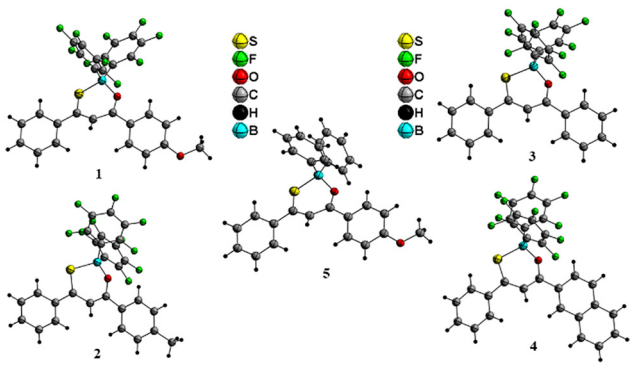

Fig. 1 X-ray crystal structure of complexes **1–5** with ball and stick model (diamond view).

$(C_6H_5)_2$ owing to the electron withdrawing nature of perfluorinated phenyl groups. Complexes with $-B(C_6F_5)_2$ motif (**1–4**) did not show any solvatochromism, however, complexes with $-B(C_6H_5)_2$ motif (**5–8**) exhibit positive solvatochromism. This result reveals that there is effective interaction between polar solvents and complexes **5–8**. As discussed in the previous section, the interaction between sulphur and boron in complexes **1–4** is strong compared to **5–8**, which plays a major role for the observed absorption maxima with change of solvent polarity in **5–8**.

To gain a better understanding of the optical properties of **1–8**, we performed time-dependent density functional theory (TD-DFT) calculations after optimizing the structures at the B3LYP/6-31g(d,p). The lowest and highest occupied molecular orbitals (LUMOs and HOMOs) of the boron complexes **1–8** are presented in Table 3. The HOMOs of **1–8** are mainly distributed over the aromatic ring attached to the keto side and the thioketonate skeleton; whereas LUMOs are distributed on both the aryl moieties and the central thioketonate ring. In general, both HOMOs and LUMOs are stabilized for $-B(C_6F_5)_2$ complexes over their respective $-BPh_2$ substituted complexes, which suggests that the electron withdrawing nature of the "pentafluorophenyl" group plays a major role for the observed values. The low LUMO values justify the observed lower reduction potential observed in **1–4** which will be discussed in the following section.

We further analysed the complexes **1–8** using fluorescence spectroscopy, which revealed that complexes **5–8** are non-fluorescent ($\phi_F \leq 0.01\%$), however, complexes **1–4** exhibit weak fluorescence (ϕ_F = 0.1 to 0.14%). This result suggests that substituents on the boron atom (C_6F_5 *vs.* C_6H_5) play a major role in the detected luminescence. The photoluminescence decay of the boron complexes **1–4** exhibited an average lifetime of 0.2–0.6 ns in dichloromethane (Table 2). Further evaluation of the DFT reveals that the lowest energy excitation for complexes **1–4** is largely HOMO to LUMO transitions, however, for complexes **5–8** it is HOMO-2 to LUMO transitions. The HOMO-2 of complexes **5–8** localized on the "phenyl" group attached to the boron center (Tables S7–S10‡). This difference may be the reason for the detected luminescence in the case of complexes **1–4**. In a similar fashion, complexes **1–4** showed solid state

Table 2 Photophysical data of complexes **1–8** at 298 K in dichloromethane

Complexes	λ_{abs} [a](nm) ($\varepsilon \times 10^4$ (M^{-1} cm^{-1}))	λ_{ems} [b] (nm)	ϕ_F [c] (%)	τ [d] (ns)
1	353 (1.5), 458 (3.0)	534	0.12	0.23
2	345 (1.8), 448 (2.2)	551	0.11	0.41
3	344 (1.9), 445 (1.9)	557	0.10	0.59
4	348 (1.8), 463 (2.7)	549	0.14	0.35
5	346 (1.6), 465 (2.1)	—	—	—
6	336 (1.7), 455 (1.3)	—	—	—
7	334 (1.5), 455 (1.0)	—	—	—
8	337 (1.6), 467 (1.6)	—	—	—

[a] Absorption maximum (conc. = 0.35 × 10^{-4} M), [b] excited at λ_{max}, [c] quantum yield measured using integrating sphere module, [d] emission lifetime.

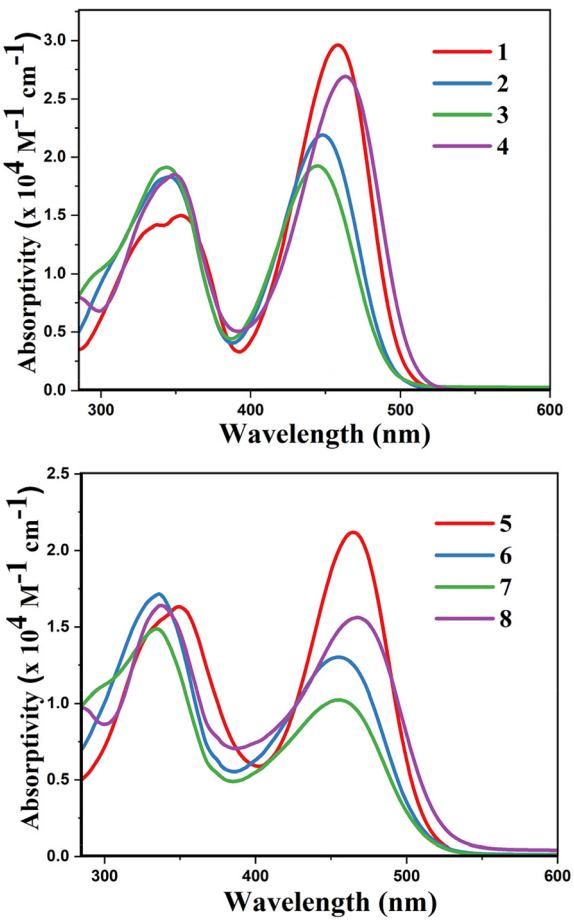

Fig. 2 Absorption spectra of boron complexes **1–4** (top) and **5–8** (down) (0.35 × 10^{-4} M) in DCM.

photoluminescence from 554–617 nm (Fig. 3), however, complexes **5–8** did not show any emission in the solid-state.

Electrochemical studies

The electrochemical properties of the complexes **1–8** were studied in N_2 bubbled dichloromethane at 298 K using cyclic

Table 3 Electronic distribution in the HOMO and LUMO state of **1–8**

Complexes	HOMO	LUMO
1	-6.212 eV	-2.910 eV
2	-6.442 eV	-2.998 eV
3	-6.539 eV	-3.046 eV
4	-6.187 eV	-3.056 eV
5	-6.132 eV	-2.811 eV
6	-6.302 eV	-2.892 eV
7	-6.361 eV	-2.941 eV
8	-6.130 eV	-2.947 eV

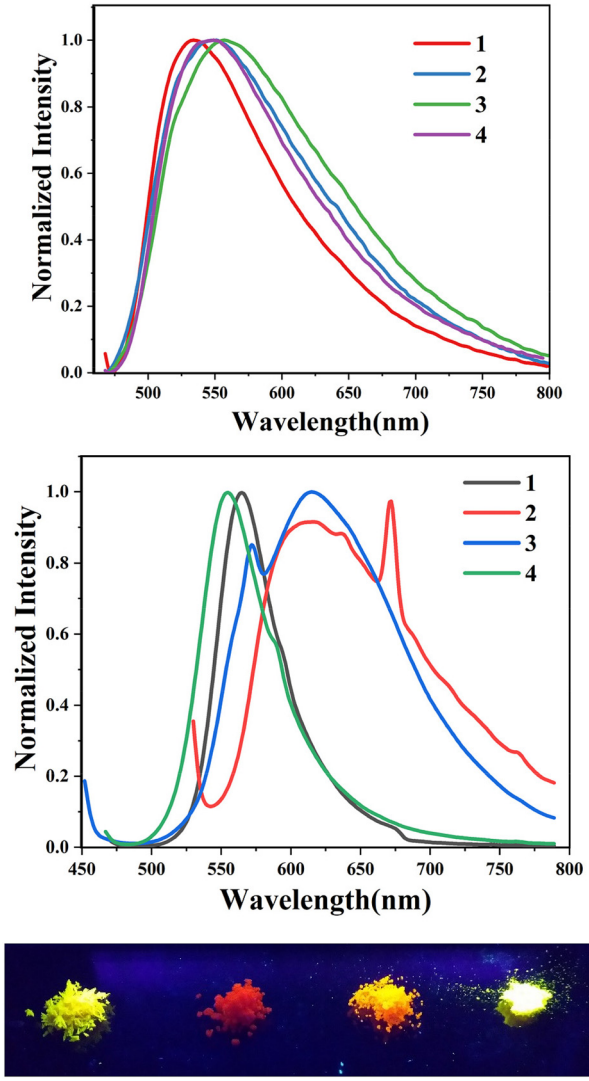

Fig. 3 (top) Photoluminescence spectra of complexes **1–4** (3.5×10^{-5} M) in CH_2Cl_2. (middle) Photoluminescence spectra of complexes **1–4** in the solid state. (bottom) Photograph of solid-state emission of complexes **1–4**.

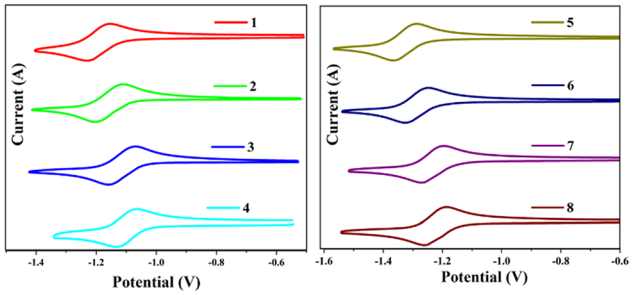

Fig. 4 Cyclic voltammogram of boron complexes **1–8** at a scan rate of 50 mV s^{-1} in dichloromethane (0.1 M of $^nBu_4N[PF_6]$ as the supporting electrolyte, *vs.* Fc/Fc^+).

Table 4 HOMO–LUMO levels calculated from electrochemical and UV-Vis absorption

Complexes	E_{pc}	E_g [a]	LUMO[b]	HOMO[c]	E_g [d]
1	−1.19	2.48	−3.44	−5.92	3.30
2	−1.15	2.49	−3.46	−5.95	3.44
3	−1.11	2.50	−3.51	−6.01	3.49
4	−1.09	2.43	−3.52	−5.95	3.13
5	−1.32	2.41	−3.39	−5.80	3.32
6	−1.28	2.40	−3.39	−5.79	3.41
7	−1.23	2.40	−3.38	−5.78	3.42
8	−1.22	2.34	−3.43	−5.77	3.18

[a] Absorption onset determined from UV low energy band. [b] Calculated from E_{pc} with reference to Fc/Fc^+. [c] Calculated from E_g and LUMO. [d] Obtained from DFT calculations. E_{pc} = cathodic peak potential. E_g = HOMO to LUMO gap.

voltammetry. All the complexes **1–8** showed one reversible reduction in the range −1.09 to −1.32 V (Fig. 4 and Table 4). The reduction potential was altered by switching the groups on the boron atom. The diphenylboron complexes (**5–8**) showed more negative potential over the bis(pentaflurophenyl) boron complexes (**1–4**). Among the four bis(pentaflurophenyl) boron complexes (**1–4**) studied, **1** exhibited a more negative value of −1.19 V owing to the presence of the –OMe group, whereas complex **4** exhibited the less negative value of −1.09 V because of the stabilized LUMO level. A similar pattern was detected for the diphenylboron complexes **5–8** ($E_{1/2}$ for **5** is −1.32 V and for **8** is −1.22 V).

Nonlinear optical measurements

The lack of exploration of substituent variation on the boron centre, motivated us to investigate the nonlinear optical properties of the boron-β-thioketonate moieties for applications in photonic limiting and switching. The nonlinear optical measurements for complexes **1–8** were carried out using the open-aperture (OA) as well as closed-aperture (CA) single-beam *Z*-scan technique, with an optimally focused ultrashort pulsed laser beam. A fiber laser emitting linearly polarized ultrashort pulses at 370 fs at a central wavelength of 1030 nm was used for the experiment. The measurements were carried out at a laser pulse repetition rate of 100 kHz that results in an on-axis peak intensity of approximately 42 GW cm^{-2} at the focus (z = 0). The detailed experimental configuration and the measurement method is elaborated in the ESI.‡ Fig. 5a presents the measured OA normalized transmittance and Fig. 5b shows the CA transmittance, for complex **1**. The OA measurement curve has a valley in the transmission signifying the nonlinear absorption which is primarily led by a two-photon absorption (TPA) process at 1030 nm excitation wavelength. On the other hand, the CA transmittance exhibits a pre-focal maximum followed by a post-focal minimum which depicts a negative sign for the nonlinear refractive index. The OA and CA *Z*-scan transmission curves for complexes **2–8** are shown in Fig. S1 and S2 in the ESI,‡ the transmittance variation for each resembles that observed in Fig. 5a and b, except for complex **6**.

The estimated values of β and n_2 are tabulated in Table 5 for all the complexes. It is apparent that most of the com-

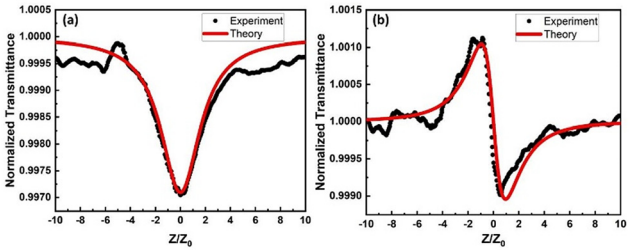

Fig. 5 Measured normalized transmittance (black dotted curve) as a function of sample position for (a) open-aperture (OA) and (b) closed-aperture (CA) *Z*-scan experiment for complex **1**. The red solid curves are theoretical fits as per eqn (S6) and (S7)‡.

Table 5 A comparative view of optical nonlinearities of various complexes

Complexes	β (cm W^{-1})	n_2 (cm^2 W^{-1})
1	1.99×10^{-12}	-2.01×10^{-17}
2	-0.61×10^{-12}	-3.19×10^{-17}
3	-0.95×10^{-12}	1.37×10^{-17}
4	-1.15×10^{-12}	-2.67×10^{-17}
5	-1.12×10^{-12}	-4.22×10^{-17}
6	1.34×10^{-12}	-1.65×10^{-17}
7	-1.60×10^{-12}	-3.91×10^{-17}
8	6.37×10^{-12}	-4.35×10^{-17}

pounds exhibit weak saturable absorption (SA) behaviour except for complexes **1**, **6**, and **8**. The UV-visible optical absorption spectrum (see Fig. 5) indicates that there should be a predominant contribution of two-photon absorption (TPA) in the reverse saturable absorption (RSA) signature for **1**, **6**, and **8**. In general, a smaller HOMO–LUMO gap renders a molecular configuration that is more susceptible to an external (exciting) electromagnetic field. In other words, the strength of hyperpolarizability would be higher for a molecule with a smaller HOMO–LUMO gap.[43,44] Amongst all the complexes, **8** exhibits the smallest HOMO–LUMO gap and consequently, the nonlinear coefficient (β) is the highest for **8**. In line with this argument, **2** and **3** are expected to exhibit weak nonlinear optical absorption (NLA) owing to a high HOMO–LUMO gap for the $S_0 \rightarrow S_1$ transition. This is indeed observed except for a negative sign which represents saturable absorption (SA) behaviour. It is surprising to observe that a majority of the complexes exhibit a weak SA signature at 1030 nm excitation wavelength. A plausible attribution could be a bulky ligand architecture that reduces the charge carrier mobility at ultrashort pulse (<400 fs) time scales. Due to this phase lag in electronic response from the molecules (**2–5**, and **7**), the nonlinear optical absorption peaks when the excitation laser intensity maximizes (z = 0). Additionally, the presence of an electron withdrawing pentafluorophenyl group in complexes **2–4** manifests as a weakened NLA. It is worth noting that the conjugation length (bond length) and the dihedral angle play a crucial role in determining hyperpolarizability in molecules. Dihedral angles close to zero or π provide a low hindrance mobility for intramolecular charge transfer and hence, this could lead to stronger hyperpolarizability in molecules.[45] It could be observed from Tables S3 and S4,‡ that complex **8** exhibits the lowest dihedral angle which manifests through a strong NLO response. It is crucial to point out that the excitation ultrashort pulses are incident at a repetition rate of approximately 100 kHz. At such a high pulse incidence rate, the impact of thermo-optic effects could be substantial in comparison with the electronic contribution to optical nonlinearity. This is apparent from the refractive optical nonlinearity (Table 5) where it could be observed that most of the complexes exhibit a self-defocusing (negative n_2) effect for the 1030 nm excitation laser.

Conclusion

In conclusion, we have prepared different O,S-chelated $B(C_6F_5)_2$ and $B(C_6H_5)_2$ substituted monothio-β-diketonates (**1–8**). Structural analysis of **1–5** realised that the B–S and B–O bond distances of the bis(pentafluorophenyl)boron complexes are notably shorter than the diphenyl boron complexes. The optical and electrochemical properties along with DFT studies of the boron complexes **1–8** were studied in detail. The diphenyl boron complexes (**5–8**) displayed red shifted absorption compared to bis(pentafluorophenyl)boron complexes (**1–4**). Further, diphenyl boron complexes exhibited a high negative potential over the bis(pentafluorophenyl)boron complexes. TD-DFT studies further showed that the HOMO–LUMO gap altered with changing moiety on the boron centre, that is phenyl *vs.* pentaflurophenyl. The nonlinear optical absorption properties of the synthesized complexes vary from a TPA-led RSA signature to an SA signature by virtue of the bulky ligand architecture. Most of the monothio-β-diketonate derivatives exhibit a self-defocusing effect owing to the strong thermo-optic contribution.

Experimental section

The starting materials **L1–L4**, the bis(pentafluorophenyl)boron monothio-β-diketonates **1–4** and diphenylboron monothio-β-diketonates **5–8** were synthesized using previously reported procedures.[17,41]

The details of the quantities involved, yields and other data are given below.

Synthesis of L1

4-Methoxyacetophenone (8.9 mmol, 1.30 g), methyl benzodithioate (10.7 mmol, 1.80 g), and NaH (19.6 mmol, 0.47 g). Yield: 60.0% (1.40 g). ^{1}H NMR (400 MHz, $CDCl_3$) δ 3.90 (s, 3H), 6.99 (d, J = 8.8 Hz, 2H). 7.39–7.52 (m, 4H), 7.81 (d, J = 8.0 Hz, 2H), 8.01 (d, J = 8.0 Hz, 2H), 15.42 (s, 1H). ^{13}C NMR (101 MHz, $CDCl_3$) δ 55.7, 110.3, 114.4, 126.9, 127.9, 128.6, 129.6, 131.0, 145.8, 163.6, 179.6, 202.0. ESI (HR-MS). Calcd for $C_{16}H_{14}O_2S$ ($[M + Na]^+$): m/z 293.0612, found: 293.0603.

Synthesis of L2

4-Methylacetophenone (8.9 mmol, 1.20 g), methyl benzodithioate (10.7 mmol, 1.80 g), and NaH (19.7 mmol, 0.47 g). Yield: 58.0% (1.30 g). ^{1}H NMR (400 MHz, $CDCl_3$) δ 2.43 (s, 3H), 7.30 (d, J = 8.0 Hz, 2H), 7.36–7.53 (m, 4H), 7.81 (d, J = 8.0 Hz, 2H), 7.92 (d, J = 8.0 Hz, 2H), 15.38 (s, 1H). ^{13}C NMR (101 MHz, $CDCl_3$) δ 21.8, 110.5, 126.9, 127.4, 128.6, 129.7, 131.1, 132.9, 143.8, 145.7, 179.9, 203.5. ESI (HR-MS). Calcd for $C_{16}H_{14}OS$ ($[M + H]^+$): m/z 255.0838, found: 255.0819.

Synthesis of L3

Acetophenone (8.9 mmol, 1.10 g), methyl benzodithioate (10.7 mmol, 1.80 g), and NaH (23.6 mmol, 0.57 g). Yield: 47.0% (1.50 g). ^{1}H NMR (400 MHz, $CDCl_3$) δ 7.61–7.40 (m, 7H), 7.79–7.89 (m, 2H), 8.02 (d, J = 8.0 Hz, 2H), 15.24 (s, 1H). ^{13}C NMR (101 MHz, $CDCl_3$) δ 110.7, 126.9, 127.3, 128.6, 129.0, 131.2, 132.7, 135.8, 145.6, 179.8, 203.6. ESI (HR-MS). Calcd for $C_{15}H_{12}OS$ ($[M + H]^+$): m/z 241.0682, found: 241.0649.

Synthesis of L4

2-Acetylnaphthalene (8.8 mmol, 1.50 g), methyl benzodithioate (10.7 mmol, 1.80 g), and NaH (19.4 mmol, 0.46 g). Yield: 62.0% (1.60 g). ^{1}H NMR (400 MHz, $CDCl_3$) δ 7.44–7.64 (m, 6H), 7.84–8.06 (m, 6H), 8.58 (s, 1H), 15.41 (s, 1H). ^{13}C NMR (101 MHz, $CDCl_3$) δ 111.0, 123.2, 127.0, 127.0, 127.9, 128.5, 128.6, 128.7, 128.8, 129.5, 131.2, 132.9, 132.9, 135.4, 145.7, 179.5, 204.0. ESI (HR-MS). Calcd for $C_{19}H_{14}OS$ ($[M + H]^+$): m/z 291.0844, found: 291.0822.

Synthesis of 1

L1 (1.5 mmol, 0.40 g) and $B(C_6F_5)_3$ (1.7 mmol, 0.90 g). Yield: 56.0% (0.50 g). ^{1}H NMR (700 MHz, $CDCl_3$) δ 3.96 (s, 3H), 7.08 (d, J = 8.0 Hz, 2H), 7.51 (t, J = 7.8 Hz, 2H), 7.59–7.64 (m, 2H), 7.89 (d, J = 8.0 Hz, 2H), 8.26 (d, J = 8.0 Hz, 2H). ^{11}B NMR (128 MHz, $CDCl_3$) δ 1.7. ^{13}C NMR (176 MHz, $CDCl_3$) δ 56.0, 110.4, 115.0, 126.1, 128.5, 129.2, 132.9, 133.6, 136.5, 137.3 (d = 262 Hz), 139.7, 140.3 (d, J = 250 Hz), 147.8 (d, J = 236 Hz), 166.2, 181.4, 188.4. ^{19}F NMR (376 MHz, $CDCl_3$) δ −163.3 (t, 4F, Pf), −156.6 (t, 2F, Pf), −134.2 (d, 4F, Pf). ESI (HR-MS). Calcd for $C_{28}H_{13}BF_{10}O_2S$ ($[M]^+$): m/z 614.0606, found: 614.0568.

Synthesis of 2

L2 (1.9 mmol, 0.50 g) and $B(C_6F_5)_3$ (2.3 mmol, 1.20 g). Yield: 67.0% (0.78 g). ^{1}H NMR (700 MHz, $CDCl_3$) δ 2.51 (s, 3H), 7.41 (d, J = 8.1 Hz, 2H), 7.53 (t, J = 8.0 Hz, 2H), 7.64 (t, J = 8.0 Hz, 1H), 7.69 (s, 1H), 7.91 (d, J = 8.0 Hz, 2H), 8.18 (d, J = 8.0 Hz, 2H). ^{11}B NMR (128 MHz, $CDCl_3$) δ 1.7. ^{13}C NMR (176 MHz, $CDCl_3$) δ 22.1, 110.7, 128.5, 129.2, 130.3, 131.0, 133.9, 137.2 (d, J = 253 Hz), 139.5, 140.4 (d, J = 250 Hz), 147.7, 147.8 (d, J = 246 Hz), 182.4, 190.4. ^{19}F NMR (376 MHz, $CDCl_3$) δ −163.2 (t, 4F, Pf), −156.4 (t, 2F, Pf), −134.2 (d, 4F, Pf). ESI (HR-MS). Calcd for $C_{28}H_{13}BF_{10}OS$ ($[M - H]^+$): m/z 597.0579, found: 597.0650.

Synthesis of 3

L3 (3.1 mmol, 0.75 g) and $B(C_6F_5)_3$ (3.7 mmol, 1.90 g). Yield: 79.0% (1.45 g). ^{1}H NMR (700 MHz, $CDCl_3$) δ 7.54 (t, J = 8.0 Hz, 2H), 7.61 (t, J = 8.0 Hz, 2H), 7.66 (t, J = 8.0 Hz, 1H), 7.69 (s, 1H), 7.74 (t, J = 8.0 Hz, 1H), 7.92 (d, J = 8.0 Hz, 2H), 8.26 (d, J = 8.0 Hz, 2H). ^{11}B NMR (128 MHz, $CDCl_3$) δ 1.8. ^{13}C NMR (176 MHz, $CDCl_3$) δ 76.9, 77.1, 77.3, 110.9, 128.6, 129.3, 129.5, 130.1, 133.6, 134.1, 135.7, 137.3 (d, J = 250 Hz), 139.4, 140.4 (d, J = 252 Hz), 147.8, 182.4, 191.8. ^{19}F NMR (376 MHz, $CDCl_3$) δ −163.1 (t, 4F, Pf), −156.3 (t, 2F, Pf), −134.2 (d, 4F, Pf). ESI (HR-MS). Calcd for $C_{27}H_{11}BF_{10}OS$ ($[M + H]^+$): m/z 584.0500, found: 584.0539.

Synthesis of 4

L4 (1.7 mmol, 0.50 g) and $B(C_6F_5)_3$ (2.1 mmol, 1.10 g). Yield: 69.0% (0.75 g). ^{1}H NMR (400 MHz, $CDCl_3$) δ 7.56 (t, J = 8.0 Hz, 2H), 7.60–7.74 (m, 3H), 7.83 (s, 1H), 7.91–8.04 (m, 4H), 8.08 (d, J = 8.0 Hz, 1H), 8.20 (d, J = 8.0 Hz, 1H), 8.85 (s, 1H). ^{11}B NMR (128 MHz, $CDCl_3$) δ 1.8. ^{13}C NMR (176 MHz, $CDCl_3$) δ 111.2, 124.4, 127.6, 128.1, 128.6, 129.3, 129.3, 130.2, 130.4, 130.9, 132.7, 132.9, 134.1, 136.8, 137.3 (J = 271 Hz), 139.6, 140.4 (d, J = 260 Hz), 147.9 (d, J = 246 Hz), 182.1, 191.2. ^{19}F NMR (377 MHz, $CDCl_3$) δ −163.1 (t, 4F, Pf), −156.3 (t, 2F, Pf), −134.1 (d, 4F, Pf). ESI (HR-MS). Calcd for $C_{31}H_{13}BF_{10}OS$ ($[M - H]^+$): m/z 633.0657, found: 633.0659.

Synthesis of 5

L1 (1.5 mmol, 0.40 g) and $B(C_6H_5)_3$ (1.7 mmol, 0.43 g). Yield: 81.0% (0.52 g). ^{1}H NMR (400 MHz, $CDCl_3$) δ 3.94 (s, 3H), 7.05 (d, J = 8.0 Hz, 2H), 7.16–7.30 (m, 6H), 7.43–7.50 (m, 3H), 7.58 (d, J = 8.0 Hz, 5H), 7.89 (d, J = 8.0 Hz, 2H), 8.27 (d, J = 8.0 Hz, 2H). ^{11}B NMR (128 MHz, $CDCl_3$) δ 6.3. ^{13}C NMR (101 MHz, $CDCl_3$) δ 55.9, 111.4, 114.7, 126.5, 127.2, 128.1, 128.9, 131.8, 132.2, 132.8, 140.6, 165.2, 180.7, 189.3. ESI (HR-MS). Calcd for $C_{28}H_{24}BO_2S$ ($[M + H]^+$): m/z 435.1626, found: 435.1591.

Synthesis of 6

L2 (1.9 mmol, 0.50 g) and $B(C_6H_5)_3$ (0.57 g, 2.4 mmol). Yield: 65.0% (0.54 g). ^{1}H NMR (400 MHz, $CDCl_3$) δ 2.49 (s, 3H), 7.15–7.31 (m, 6H), 7.37 (d, J = 8.0 Hz, 2H), 7.48 (d, J = 8.0 Hz, 2H), 7.53–7.63 (m, 6H), 7.88–7.95 (m, 2H), 8.18 (d, J = 8.0 Hz, 2H). ^{11}B NMR (128 MHz, $CDCl_3$) δ 6.1. ^{13}C NMR (101 MHz, $CDCl_3$) δ 22.1, 111.6, 126.6, 127.2, 128.1, 128.9, 129.3, 130.1, 132.2, 133.0, 140.5, 146.2, 181.4, 191.0. ESI (HR-MS). Calcd for $C_{28}H_{23}BOS$ ($[M]^+$): m/z 418.1677, found: 418.1649.

Synthesis of 7

L3 (2.0 mmol, 0.50 g) and $B(C_6H_5)_3$ (2.5 mmol, 0.60 g). Yield: 54.0% (0.46 g). ^{1}H NMR (700 MHz, $CDCl_3$) δ 7.22 (d, J = 8.0 Hz, 2H), 7.24–7.29 (m, 4H), 7.48 (t, J = 7.8 Hz, 2H), 7.53–7.63 (m, 8H), 7.69 (d, J = 8.0 Hz, 1H), 7.91 (d, J = 8.0 Hz, 2H), 8.26 (d, J = 8.0 Hz, 2H). ^{11}B NMR (128 MHz, $CDCl_3$) δ 5.0. ^{13}C NMR (176 MHz, $CDCl_3$) δ 111.7, 126.7, 127.3, 128.2, 129.0, 129.1, 129.3, 132.2, 133.2, 134.6, 134.9, 140.4, 181.4, 192.2. ESI

(HR-MS). Calcd for $C_{27}H_{22}BOS$ ($[M + H]^+$): m/z 405.1521, found: 405.1511.

Synthesis of 8

L4 (1.7 mmol, 0.50 g) and $B(C_6H_5)_3$ (2.0 mmol, 0.5 g). Yield: 67.0% (0.52 g). ^{1}H NMR (400 MHz, $CDCl_3$) δ 7.21–7.37 (m, 6H), 7.54 (t, J = 7.6 Hz, 2H), 7.61–7.75 (m, 8H), 7.95–8.05 (m, 4H), 8.09 (d, J = 8.0 Hz, 1H), 8.27 (d, J = 8.0 Hz, 1H), 8.90 (s, 1H). ^{11}B NMR (128 MHz, $CDCl_3$) δ 5.2. ^{13}C NMR (101 MHz, $CDCl_3$) δ 112.1, 124.1, 126.7, 127.3, 127.4, 128.0, 128.2, 129.0, 129.1, 129.5, 130.1, 131.3, 132.1, 132.3, 132.9, 133.1, 136.3, 140.5, 181.1, 191.8. ESI (HR-MS). Calcd for $C_{31}H_{24}BOS$ ($[M + H]^+$): m/z 455.1677, found: 455.1630.

Author contributions

The manuscript was written through contributions from all authors. All authors have given approval to the final version of the manuscript.

Data availability

Crystallographic data for **1–5** have been deposited at the CCDC under 2380850–2380854. All other data supporting this article have been included as part of the ESI.‡

Conflicts of interest

There are no conflicts to declare.

Acknowledgements

KV thanks the Department of Atomic Energy (DAE) and Science and Engineering Research Board (SERB) (CRG/2023/000085) for financial support. ACM thanks NISER for the fellowship. This manuscript is adapted from Dr Anna Chandrasekar Murali's dissertation, National Institute of Science Education and Research (NISER), an OCC of Homi Bhabha National Institute, India, 2023.

References

1 K. Liu, R. A. Lalancette and F. Jäkle, *J. Am. Chem. Soc.*, 2017, **139**, 18170–18173.
2 J. Huang and Y. Li, *Front. Chem.*, 2018, **6**, 341–363.
3 C. C. Vidyasagar, B. M. Munoz Flores, V. M. Jimenez-Perez and P. M. Gurubasavaraj, *Mater. Today Chem.*, 2019, **11**, 133–155.
4 D. Franz and S. Inoue, *Chem. – Eur. J.*, 2019, **25**, 2898–2926.
5 K. Liu, R. A. Lalancette and F. Jäkle, *J. Am. Chem. Soc.*, 2019, **141**, 7453–7462.
6 S. Bellinger, M. Hatamimoslehabadi, R. E. Borg, J. La, P. Catsoulis, F. Mithila, C. Yelleswarapu and J. Rochford, *Chem. Commun.*, 2018, **54**, 6352–6355.
7 M. Hayakawa, M. Kameda, R. Kawasumi, S. Nakatsuka, N. Yasuda and T. Hatakeyama, *Angew. Chem., Int. Ed.*, 2023, **62**, e202217512.
8 J. Shi, Z. Ran and F. Peng, *Dyes Pigm.*, 2022, **204**, 110383.
9 A. C. Murali, P. Nayak and K. Venkatasubbaiah, *Dalton Trans.*, 2022, **51**, 5751–5771.
10 X. Chen, D. Tan and D.-T. Yang, *J. Mater. Chem. C*, 2022, **10**, 13499–13532.
11 J. Gong and X. Zhang, *Coord. Chem. Rev.*, 2022, **453**, 214329.
12 V. Mukundam, S. Sa, A. Kumari, T. Teja Ponduru, R. Das and K. Venkatasubbaiah, *Chem. – Asian J.*, 2022, **17**, e202200291.
13 P. Nayak, A. C. Murali, V. Chandrasekhar and K. Venkatasubbaiah, *Mater. Adv.*, 2022, **3**, 5893–5899.
14 S. Sa, A. Sahoo, S. Mukherjee, A. Perumal and K. Venkatasubbaiah, *Dyes Pigm.*, 2022, **206**, 110585.
15 X. Li, G. Zhang and Q. Song, *Chem. Commun.*, 2023, **59**, 3812–3820.
16 R. Kannan, P. Nayak, R. Arumugam, D. Krishna Rao, K. R. Mote, A. C. Murali, K. Venkatasubbaiah and V. Chandrasekhar, *Dalton Trans.*, 2023, **52**, 16829–16840.
17 A. C. Murali, P. Nayak, S. Nayak, S. Das, S. P. Senanayak and K. Venkatasubbaiah, *Angew. Chem., Int. Ed.*, 2023, **62**, e202216871.
18 A. C. Murali, P. Pratakshya, P. Patel, P. Nayak, S. Peruncheralathan and K. Venkatasubbaiah, *New J. Chem.*, 2023, **47**, 17835–17842.
19 C. Jin, X. Yang, W. Zhao, Y. Zhao, Z. Wang and J. Tan, *Coord. Chem. Rev.*, 2024, **513**, 215892.
20 P. Nayak, S. Mukherjee, D. Patel, A. A. Mahapatra, A. C. Murali, A. Perumal and K. Venkatasubbaiah, *ACS Appl. Opt. Mater.*, 2024, **2**, 1523–1532.
21 P.-Z. Chen, L.-Y. Niu, Y.-Z. Chen and Q.-Z. Yang, *Coord. Chem. Rev.*, 2017, **350**, 196–216.
22 M. V. Filippov, Y. N. Kononevich, D. S. Ionov, A. A. Safonov, A. I. Karnaeva, V. A. Sazhnikov, M. V. Alfimov and A. M. Muzafarov, *ChemPhotoChem*, 2024, **8**, e202300317.
23 S. Ito, M. Gon, K. Tanaka and Y. Chujo, *Natl. Sci. Rev.*, 2021, **8**, nwab049.
24 P. Xue, X. Wang, W. Wang, J. Zhang, Z. Wang, J. Jin, C. Zheng, P. Li, G. Xie and R. Chen, *ACS Appl. Mater. Interfaces*, 2021, **13**, 47826–47834.
25 M. L. Daly, C. Kerr, C. A. DeRosa and C. L. Fraser, *ACS Appl. Mater. Interfaces*, 2017, **9**, 32008–32017.
26 C. A. DeRosa, M. Kolpaczynska, C. Kerr, M. L. Daly, W. A. Morris and C. L. Fraser, *ChemPlusChem*, 2017, **82**, 399–406.
27 C. Kerr, C. A. DeRosa, M. L. Daly, H. Zhang, G. M. Palmer and C. L. Fraser, *Biomacromolecules*, 2017, **18**, 551–561.
28 F. Wang, C. A. De Rosa, M. L. Daly, D. Song, M. Sabat and C. L. Fraser, *Mater. Chem. Front.*, 2017, **1**, 1866–1874.
29 C.-L. Wong, C.-T. Poon and V. W.-W. Yam, *Organometallics*, 2017, **36**, 2661–2669.

30 T. Butler, M. Zhuang and C. L. Fraser, *J. Phys. Chem. C*, 2018, **122**, 19090–19099.
31 T. Liu, G. Zhang, R. E. Evans, C. O. Trindle, Z. Altun, C. A. De Rosa, F. Wang, M. Zhuang and C. L. Fraser, *Chem. – Eur. J.*, 2018, **24**, 1859–1869.
32 J. Sun, C. Qian, S. Xu, X. Jia, L. Zhai, J. Zhao and R. Lu, *Org. Biomol. Chem.*, 2018, **16**, 7438–7445.
33 R. Jimenez, F. Duarte, S. Nuti, J. A. Campo, C. Lodeiro, M. Cano and C. Cuerva, *Dyes Pigm.*, 2020, **177**, 108272.
34 P. Li, Q. Liang, E. Y.-H. Hong, C.-Y. Chan, Y.-H. Cheng, M.-Y. Leung, M.-Y. Chan, K.-H. Low, H. Wu and V. W.-W. Yam, *Chem. Sci.*, 2020, **11**, 11601–11612.
35 M. Zhuang, S. Joshi, H. Sun, T. Batabyal, C. L. Fraser and J. Kapur, *Sci. Rep.*, 2021, **11**, 1076.
36 X. Wang, G. Wang, J. Li, X. Li and K. Zhang, *Polymer*, 2022, **239**, 124449.
37 D.-H. Kim, A. D'Aléo, X.-K. Chen, A. D. S. Sandanayaka, D. Yao, L. Zhao, T. Komino, E. Zaborova, G. Canard, Y. Tsuchiya, E. Choi, J. W. Wu, F. Fages, J.-L. Brédas, J.-C. Ribierre and C. Adachi, *Nat. Photonics*, 2018, **12**, 98–104.
38 R. Aoki, R. Komatsu, K. Goushi, M. Mamada, S. Y. Ko, J. W. Wu, V. Placide, A. D'Aléo and C. Adachi, *Adv. Opt. Mater.*, 2021, **9**, 2001947.
39 K. Tanaka, M. Gon, S. Ito, J. Ochi and Y. Chujo, *Coord. Chem. Rev.*, 2022, **472**, 214779.
40 F. P. Macedo, C. Gwengo, S. V. Lindeman, M. D. Smith and J. R. Gardinier, *Eur. J. Inorg. Chem.*, 2008, **20**, 3200–3211.
41 A. C. Murali, P. Nayak, R. Panda, R. Das and K. Venkatasubbaiah, *ACS Appl. Opt. Mater.*, 2023, **1**, 1033–1042.
42 A. Nagai, K. Kokado, Y. Nagata, M. Arita and Y. Chujo, *J. Org. Chem.*, 2008, **73**, 8605–8607.
43 M. Rodríguez, R. Castro-Beltrán, G. Ramos-Ortiz, J. L. Maldonado, N. Farfán, O. Dománguez, J. Rodríguez, R. Santillan, M. A. Meneses-Nava, O. Barbosa-García and J. Peon, *Synth. Met.*, 2009, **159**, 1281–1287.
44 Z. Yuan, N. J. Taylor, R. Ramchandran and T. B. Marder, *Appl. Organomet. Chem.*, 1996, **10**, 305–316.
45 V. Mukundam, S. Sa, A. Kumari, R. Das and K. Venkatasubbaiah, *J. Mater. Chem. C*, 2019, **7**, 12725–12737.